The human olfactory bulb processes odor valence representation and cues motor avoidance behavior

Behzad Iravani[a] (ID), Martin Schaefer[a] (ID), Donald A. Wilson[b,c], Artin Arshamian[a,d,1], and Johan N. Lundström[a,e,f,g,1,2] (ID)

[a]Department of Clinical Neuroscience, Karolinska Institutet 17177 Stockholm, Sweden; [b]Nathan Kline Institute for Psychiatric Research, Orangeburg, NY 10962; [c]Department of Child and Adolescent Psychiatry, New York University Langone Medical School, New York, NY 10016; [d]Department of Psychology, Stockholm University 10405 Stockholm, Sweden; [e]Monell Chemical Senses Center, Philadelphia, PA 19104; [f]Department of Psychology, University of Pennsylvania, Philadelphia, PA 19104; and [g]Stockholm University Brain Imaging Centre, Stockholm University 11415 Stockholm, Sweden

Determining the valence of an odor to guide rapid approach–avoidance behavior is thought to be one of the core tasks of the olfactory system, and yet little is known of the initial neural mechanisms supporting this process or of its subsequent behavioral manifestation in humans. In two experiments, we measured the functional processing of odor valence perception in the human olfactory bulb (OB)—the first processing stage of the olfactory system—using a noninvasive method as well as assessed the subsequent motor avoidance response. We demonstrate that odor valence perception is associated with both gamma and beta activity in the human OB. Moreover, we show that negative, but not positive, odors initiate an early beta response in the OB, a response that is linked to a preparatory neural motor response in the motor cortex. Finally, in a separate experiment, we show that negative odors trigger a full-body motor avoidance response, manifested as a rapid leaning away from the odor, within the time period predicted by the OB results. Taken together, these results demonstrate that the human OB processes odor valence in a sequential manner in both the gamma and beta frequency bands and suggest that rapid processing of unpleasant odors in the OB might underlie rapid approach–avoidance decisions.

olfactory bulb | valence | electrobulbogram | pleasantness | avoidance

The survival of any organism is dependent on approach–avoidance mechanisms: avoiding dangerous and approaching rewarding stimuli. Among our senses, the olfactory system seems specifically tuned to aid approach–avoidance decisions and, in particular, to assist in avoiding potentially dangerous stimuli. It is not surprising then that the very first stage of the central olfactory system, the olfactory bulb (OB), processes various information directly related to whether an odor should be avoided (1).

In nonhuman animals, the OB demonstrates rapid plasticity to aversive stimuli (1) and has dedicated processing of odors innately associated with threats (2). Sensory systems are normally attuned to signals indicating negative outcomes for the individual given that a failure to respond to such stimuli may lead to fatal consequences (3). For example, fast responses are arguably more important when withdrawing from toxic fumes than the need for speed when approaching positive odor sources. The perceptual equivalent to the motor-driven approach–avoidance system in the olfactory system is the subjective perceptual experience of an odorant's valence. Here, perceived unpleasantness of odorants emitted from potentially dangerous sources, such as, for example, rotten food, is translated to avoidance (4). However, the underlying neural mechanism for this system is largely unknown. There are two major reasons for this. First, it is difficult to assess the subjective experience of a novel odorant's valence in animal models. Second, although assessing subjective measurements from humans is straightforward, until recently, there has been no method that allows a noninvasive measure of neural signals from the human OB. With that said, several brain imaging studies on humans have targeted the central processing mechanisms underlying

valence perception. Here, valence perception has mainly been localized to the orbitofrontal cortex (OFC); cf. ref. 5. However, the OFC is an area that is situated relatively late in the central olfactory processing stream (6) and the location of neural processing of odor avoidance in nonhuman animals has been identified to be much earlier in the pathway, just one synapse away from the odor receptors in the OB (7, 8). Thus, it is necessary to study the OB to establish the underlying neural mechanism of the earliest processing stages to understand how the olfactory system processes the subjective valence of an odorant, the first stage of an approach–avoidance decision.

Based on past studies in nonhuman animals (8), we hypothesized that the OB in awake humans would demonstrate early valence-differential processing and induce a preparatory motor approach/avoidance response according to perceived odor valence. In Experiment 1, we determined whether odor valence is processed by the human OB by means of a recently developed method that allows a direct but noninvasive measurement of the human OB (9). We found that subjective odor valence could be linked to gamma and beta activity in the human OB, independent of respiration, and that an early beta activity in OB processing was linked to motor cortex processing in a valence-dependent manner. Based on these results, in Experiment 2, we assessed whether humans, akin to nonhuman

Significance

Whether an odor's perceived valence induces an approach response or triggers avoidance is critical for survival, and yet little is known about the neural mechanisms supporting this decision. Using electrophysiological measures from the human olfactory bulb (OB), the first processing stage of the olfactory system, and measures of full-body movement, we provide evidence that this process is initiated in the human OB. We demonstrate that odor valence is associated with both gamma and beta activity in the OB. Furthermore, we show that unpleasant odors have privileged temporal OB access, as indicated by early beta activity that is linked to a preparatory neural motor response in the motor cortex, which, in turn, is associated behaviorally with a fast full-body avoidance response.

animals (10), demonstrate a rapid, full-body approach/avoidance response to odors in a valence-dependent manner in the time period predicted by Experiment 1. We found that participants rapidly moved away from a negative odor source. Interestingly, only unpleasant odors produced a consistent motor response, and, importantly, this response aligned temporally with the valence-associated activity in the OB demonstrated in Experiment 1.

Results

Early Phase–Amplitude Coupling between Beta and Gamma in OB. Odor-evoked neural signals in response to six odors with varying valence were recorded from 4 electrodes located directly above the eyebrows, which, in combination with 64 electroencephalogram (EEG) scalp electrodes, were used to extract source space electrobulbogram (EBG) (9) signals from the OB (Fig. 1*A*). Inhalation phase-locked odor stimuli were delivered using a sniff-triggered, computer-controlled, and temporally precise olfactometer (11). Odor delivery delay (~200 ms) was measured with a photoionization detector and adjusted for in all analyses (12). After each odor stimulus, participants rated perceived odor intensity, valence, and familiarity. A total of 19 participants participated in 3 separate and seemingly identical sessions, comprising a total of 540 trials per participant. Next, we removed trials with artifacts including muscle and blink (see *Methods* for details) by which an average of 27.92 ± 10.49 clean trials per odor were included in the analysis for each individual. Hence, considering all six odors, the total number of trials for each individual included in our analyses was on average 167.52 ± 25.81. More importantly, there was no statistical difference

between the number of trials across odors, $F(5, 108) = 0.39$, $P > 0.86$, indicating that after artifact rejection, the experimental design remained balance.

We have previously established that the EBG measure is a valid and reliable measure of OB processing (9), but prior to our main analysis, we estimated the quality and spatial dispersion of the reconstructed OB signal within this unique dataset. To this end, we used a simulation where the spatial dispersion of three levels of signal-to-noise-ratio were assessed, namely a hypothetical ideal, the empirical level, and twofold lower (i.e., twofold larger noise level) than empirical level. This analysis confirmed that our source reconstruction method can successfully isolate OB's EBG signal in source space given that the spatial gain was similar to the hypothetical ideal condition when assessing a signal-to-noise ratio similar to what we empirically observed in the current dataset (*SI Appendix*, Fig. S1).

To allow direct comparisons between neural and behavioral data, we used representational similarity analysis (RSA)—a multivariate method that compares similarity (e.g., correlation) matrices between continuous relationships to determine the representational geometry on the individual level (13), therefore allowing direct comparisons between different parameters without being hindered by difference in scaling and other inherent differences between measuring techniques. In this case, we assess how well a perceptual feature can be decoded from neural activity (presented as degree of similarity between measures' representational dissimilarity matrix [RDM]). The perceptual and neural population RDMs were initially derived on the individual level as relationship-distances between individual odors, separately for perceptual and neural space, and later assessed for similarities between them in group-level analysis (14). In
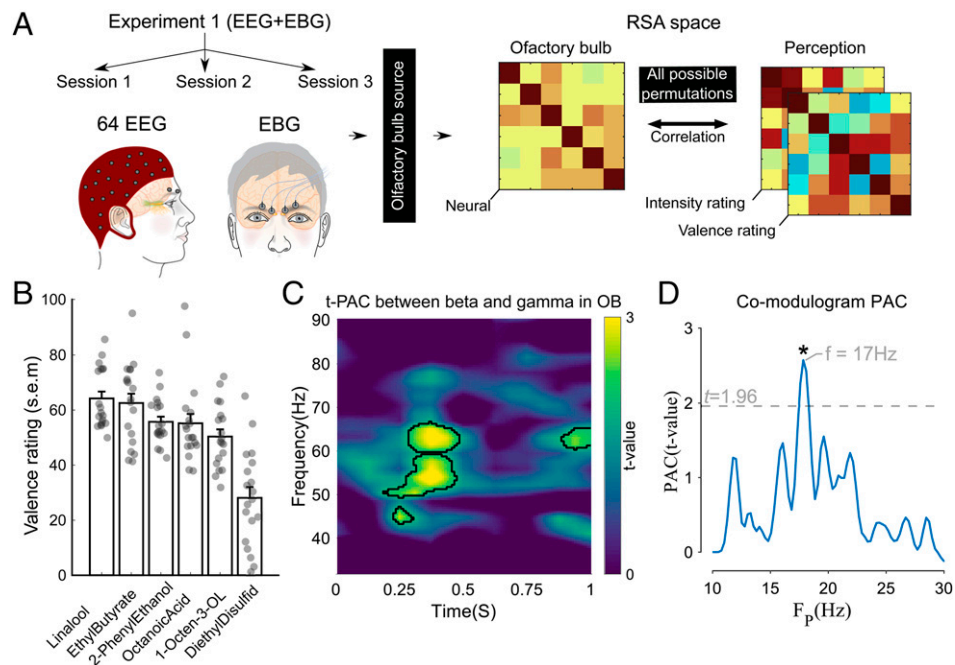

Fig. 1. Early PAC between beta and gamma in the OB. (*A*) Methodological summary of Experiment 1, where individuals (*n* = 19) were tested during three separate sessions that were subsequently merged. Source reconstruction was performed using the EEG/EGB electrodes in combination with a multi-spherical head model and digitalized electrode positions to extract OB time course. RDMs were constructed for both OB neural signals and perceptual ratings; subsequent partial Pearson correlations were derived for each time point from all possible permutations. (*B*) Group mean perceived valence ratings of the six odors in Experiment 1. Individuals' mean ratings are indicated with filled circles. Note that for analyses, valence ratings of each individual were used to create a common structure with the DISTATIS method (14). Error bars represent SEM. (*C*) Heat map showing the strength of PAC as function of time. Compared to background, a significant coupling around 53 to 65 Hz (significant results assessed with permutation testing and marked with black boundaries) starts around 250 ms after odor onset. (*D*) The comodulogram between the beta and gamma bands (~53 to 65 Hz) during the whole 1 s indicates that the coupling appeared in the beta band around ~16 to 18 Hz. Significant peak marked with asterisk and assessed with Student's *t* test. The statistical threshold for detecting significance (*t* = 1.96 equal to *P* < 0.05) is marked with a gray dashed line. F_P denotes frequency of slower oscillation or frequency phase.

other words, for each time point in the OB recording, we assess whether the relationship between the six tested odors in the neural space is similar to the relationship between ratings of the same odors in the perceptual space. Statistical relationships are then assessed for the group. Specifically, we compared how odor-induced neural activity in the OB within the gamma and beta bands corresponds to individual valence ratings of the same odors (Fig. 1*B*).

We initially assessed the relationship between activity of the beta and gamma frequency bands, determining the frequencies coupled together in OB and later the activity of these frequencies to perceived valence in RSA. Phase–amplitude coupling (PAC), a subclass of cross frequency-coupling phenomena, has been identified as a neural mechanism detectable in most mammals and critical for information processing in a multitude of brain regions (15–20). Here, the phase of the lower frequency oscillation drives the power of the coupled higher frequency oscillation. Different functional roles have been attributed to PAC, including sensory signal detection (21), executive functions (22), and attentional selection (23). Specifically for olfaction, it has recently been demonstrated that PAC in the OB shapes early sensory processing in mice (24). Given this, we examined PAC between beta and gamma oscillation within the OB and its relation to the processing of the individual's odor valence using RSA. To gain a temporal dimension of the PAC, we used time-resolved PAC [t-PAC (25)], a method that also incorporates the temporal dynamic of the signal.

As a first step, we assessed the relationship between beta and gamma bands with t-PAC within the first second after receiving an odor stimulus to determine whether these frequency bands demonstrate PAC and, if so, at which frequencies. We found significant PAC between beta and gamma already at 250 ms after odor onset (∼53 to 65 Hz), as assessed by Monte Carlo permutation test (Fig. 1*C*; $t = 3.85$, $P < 0.006$, and CI = [0.002, 0.006]). Next, we assessed the comodulogram between beta and the detected range in gamma oscillations to isolate frequencies of interest in the beta band. We found that this coupling operates in the beta band within 16 to 18 Hz ($t = 2.57$, $P < 0.009$, CI = [0.002, 0.012]; Fig. 1*D*). The t-PAC and the comodulogram results guided our subsequent neuronal and valence RSA analysis by isolating signals of interest.

Early Gamma and Late Beta Activity Relate to Perceived Odor Valence. Bandpassed OB reconstructed time courses were transformed into a complex signal using Hilbert transform. Both amplitude as well as phase were used to construct neural and perceptual valence RDMs. This was performed at each time point separately for each frequency band (gamma/beta) using the Euclidean distance across six odors that varied in valence, resulting in a sequence of RDMs (Fig. 1*A*). Then, maximum partial Pearson correlations were calculated by an approximate 80-ms-wide nonoverlapping sliding window, sweeping 0 to 1 s after odor onset anchored to inhalation, between two sequences of RDMs (Fig. 2*A*). This resulted in a correlation time course while controlling for perceived intensity (Fig. 2*B*). To test the significance of the correlation at each time point controlling for false positives, we performed a nonparametric permutation test by which all possible combinations (number of randomizations = 720) were tested for all time points ($n = 13$) during 1 s and exact P values were computed. We found time points of significant associations in RSA space between subband of gamma activity (53 to 65 Hz, consequent to PAC result) and perceived odor valence around 250 to 325 ms ($r_1 = 0.60$, $p_1 < 0.010$, CI = [0.56, 1]) (Fig. 2*B*; adjusted for measured olfactometer delay). The distribution and exact P value for the significant instance is shown in Fig. 2*C*.

Given the association between gamma activity and perceived valence, as well as the coupling between gamma amplitude and

phase of beta in the t-PAC analysis, we subsequently assessed the potential relationship between beta band and perceived valence using RSA. The extracted time course of OB was band-passed to align with the results from the previously mentioned comodulogram PAC (16 to 18 Hz). Similar to gamma, beta oscillation values were extracted and converted into complex signals using Hilbert transform to estimate instantaneous amplitude and phase values. This was next transformed to RDMs and partial Pearson correlations were performed between beta RDMs and valence RDM while controlling for perceived odor intensity, in a similar manner as described previously.

We found that there was a significant association between beta activity and valence in a time interval around ∼800 ms after odor onset (Fig. 2*D*). In other words, there was an association between variance in perceived odor valence and variance in beta activity around 800 ms after odor onset in a subband around 16 to 18 Hz. Similar to the gamma activity analysis, we tested the statistical significance of the correlations using all possible permutation tests for each time point within 1 s after odor onset. Next, we compared each actual correlation with the distribution derived from the permutation to extract the exact P value ($r = 0.65$, $P < 0.014$, CI = [0.59, 1]). The distribution and exact P value for the significant instance is shown in Fig. 2*D*.

Behavioral studies in humans have demonstrated intensity-dependent regulation of the sniff response amplitude as early as 160 ms after odor onset (26), and there are demonstrated links between sniff magnitudes and both odor valence (27) as well as odor intensity (28). Similarly, sniff rhythms have been demonstrated to regulate OB gamma oscillation in anesthetized rodents (29). Therefore, to determine whether the discovered link between valence ratings and OB activity is potentially mediated by participants' sniff patterns, unrelated to the odor presented, we assessed potential relationships between gamma and beta activity and relevant sniff parameters (sniff trace, i.e., amplitudes over time; maximum sniff amplitude; and area under the curve) using separate Spearman rank correlations. However, our analysis demonstrated that there were no significant relationships between sniff trace and OB activity in either the gamma or beta bands (*SI Appendix*, Fig. S2).

Next, we asked whether there were any commonalities in the neural representations of odor valence in the aforementioned identified gamma and beta bands. To this end, the group-level distance matrices of gamma and beta (RDMs) at the identified time periods were scaled down using the first two eigenvectors (principal component [PC]) to create two-dimensional (2D) representations. For the gamma band, valence seemed to be somewhat linearly organized along the first PC (PC1), whereas there was no obvious valence-dependent organization along the second PC axis (PC2) (Fig. 3*A*). For the beta band, there was a reverse relationship as well as a linear linkage between valence organization between the PC1–PC2 dimensions. To investigate statistically which frequency band best explained most of the individual's valence ratings, we first determined whether the organization of the odors within the 2D projections formed clusters. To this end, the RDMs were first converted to similarity matrices and communities were evaluated using a Newman algorithm (30). Odor valence ratings were hierarchically clustered from one to six clusters, and we found the elbow of modularity index (Q) graph at three, which indicates that a three-cluster solution best explains valence ratings (Fig. 3*B*). On the neural data, we subsequently derived a modularity index (Q) for each of the gamma and beta correlation peaks given the three clusters determined by hierarchical clustering of valence ratings and normalized their values to a corresponding null model from 5,000 random rewirings (31). We found that the beta band had a larger Q-value than the gamma band, meaning that the odors formed the most coherent pleasant and
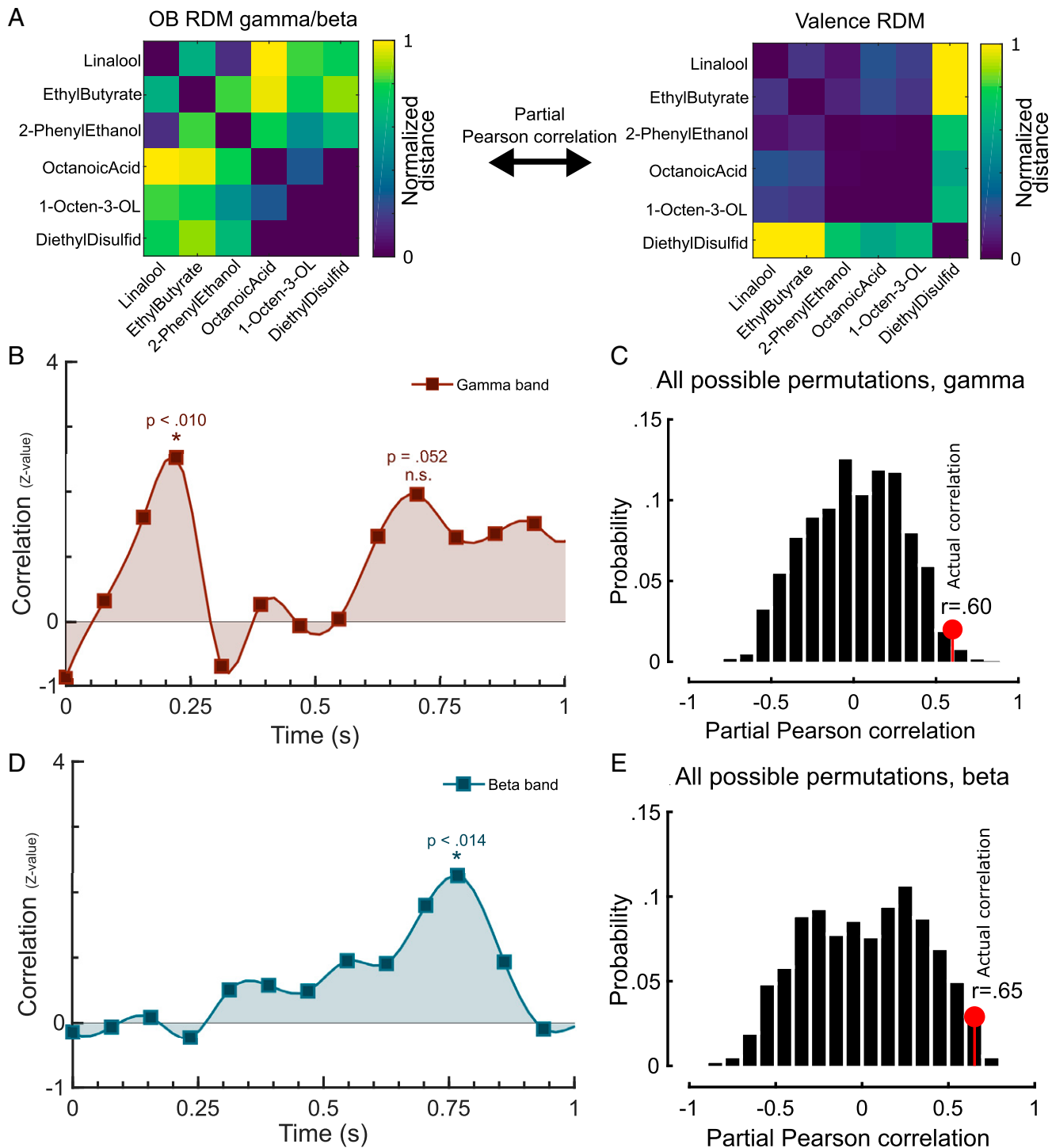
Iravani et al.
The human olfactory bulb processes odor valence representation and
cues motor avoidance behavior

PNAS | **3 of 12**
https://doi.org/10.1073/pnas.2101209118

Fig. 2. OB activity in the gamma and beta band relates to valence perception. (*A*) Example of relationships between valence and OB activity in RSA space. (*B*) Partial Pearson correlation time course between activity of gamma and valence on the group level. All possible permuted partial Pearson correlation of gamma activity and valence indicated significant correlations at a time point ~250 to 325 ms after odor onset (*P* < 0.010). (*C*) Distribution of all possible permutations for the significant instances and actual correlation indicated with red closed circles. (*D*) Correlation time course of beta activity in the OB and odor valence RDMs indicating a significant relationship with valence perception around 800 ms after odor onset. (*E*) Distribution of all possible permuted partial Pearson correlation of beta activity and valence ratings for time points centered around 800 ms (*P* < 0.014). Red closed circle shows the actual correlation within the permutation distribution.

unpleasant clusters here. This indicates that more detailed information of participants' subjective valence ratings can be obtained from the beta frequency band rather than the gamma band (Fig. 3*C*). We then statistically assessed whether the obtained modularity indexes were significantly different from

the null model using 5,000 Monte Carlo permutations tests. We found that the modularity index for beta was significantly larger than for gamma ($Z = 2.95$, $P < 0.003$, CI = [0.009, 0.018]).

These results suggest that the final odor valence perception can best be explained by processing in the beta band. Our analyses so
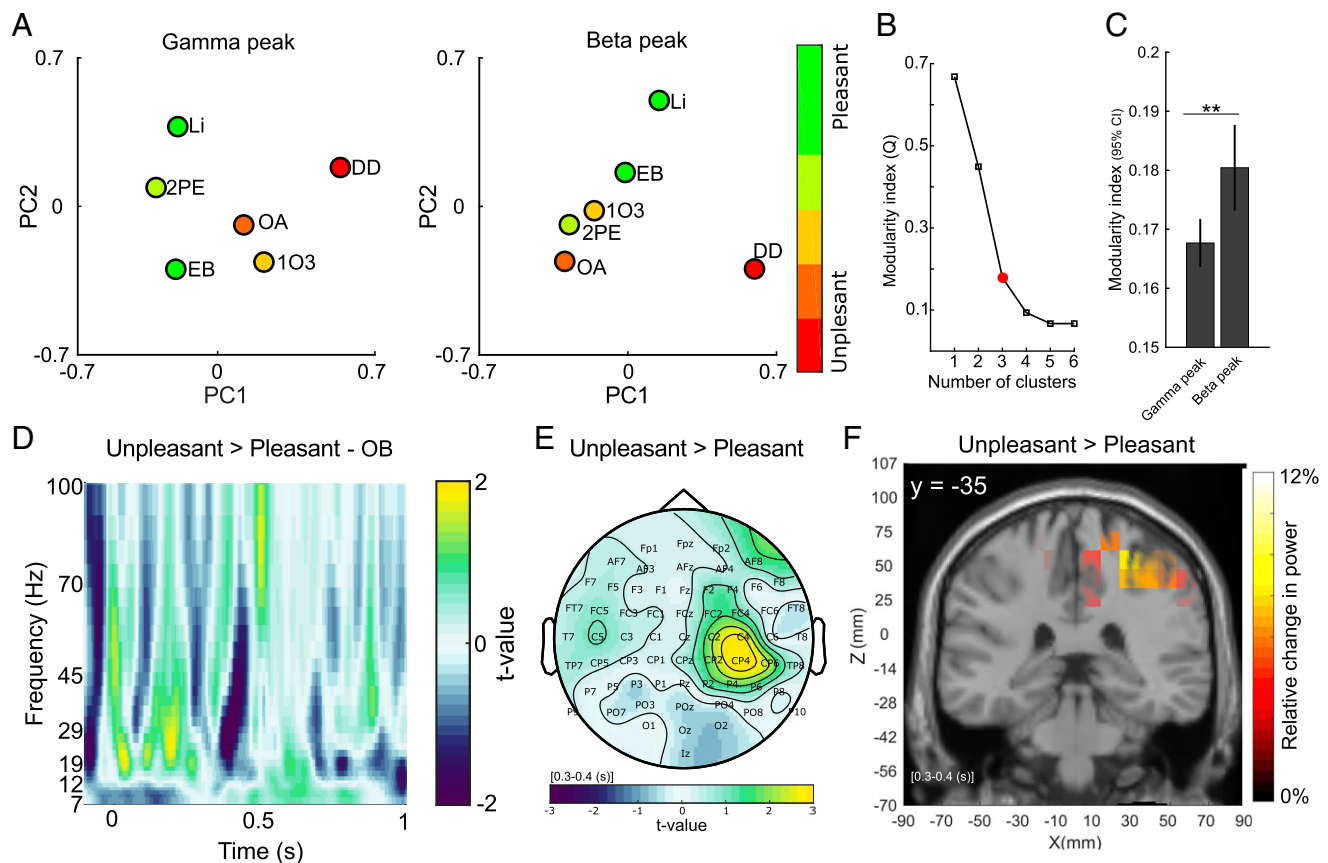
Iravani et al.
The human olfactory bulb processes odor valence representation and
cues motor avoidance behavior

Fig. 3. OB activity in the late-occurring beta band is more similar to subsequent perceptual ratings than activity in the early-occurring gamma band. (*A*) Odors placed within the 2-dimensional PC space, derived from peak values within detected significant peaks in Fig. 1 *B* and *D*, separated by frequency band. Observe the linear alignment between perceived odor valence and placement in PC space for the beta band. Odor names are written using abbreviations: Li (linalool), 2PE (2-phenyl ethanol), EB (ethyl butyrate), 1O3 (1-octen-3-ol), and DD (diethyl disulfide). Color code indicates average perceived valence where green colors denote positive valence and red/yellow colors denote negative valence. See Fig. 1*B* for absolute valence ratings. (*B*) Hierarchical clustering valence rating from 1 to 6 clusters. The elbow of the graph is shown with a red closed circle. (*C*) Newman modularity index demonstrates that mean Q-values are larger for beta synchronization, indicating that a more detailed odor valence readout can be inferred from this time point. Error bar shows 95% CI for 5,000 permutations, and ** in *C* indicates $P < 0.01$. (*D*) t-contrast map indicated more beta power during early time points and less beta power during late time points for the two most unpleasant odors compared to two most pleasant odors. (*E*) Topographical map of mu rhythm illustrates higher values for unpleasant compared to pleasant odors over motor cortex during intervals of 300 to 400 ms. (*F*) Source of mu rhythm was localized to the right motor cortex (x 27, y −35, z 60) using eLORETA during the time interval displayed in *E*, i.e., 300 to 400 ms after odor onset.

far have, however, assessed odor valence by forcing ratings into a single continuous dimension or into three clusters and used these continuous parameters to assess organizational relationships between odor perception and neural activity. This approach means that we cannot assess whether either one of the contrasting valence dimensions (pleasant or unpleasant) contribute more to the OB processing. It has been argued that positive and negative valence is separated in a 2D space (32), and a common approach in past studies has been to assess valence using a dichotomized design where groups of odors that differ in their rated valence (labeled as pleasant and unpleasant) are contrasted. To facilitate an assessment of whether there are differences in processing between pleasant and unpleasant odor in the OB, we compared OB processing of the two most pleasant odors against the two most unpleasant odors, eliminating the two neutral middle odors, all based on the individual's own valence rating. When contrasting the two odor valence categories, we found that negative odors produced a greater synchronization response in the early portion of the beta band (around 50 to 200 ms, $t = 3.01$, $P < 0.004$, probability CI range = 0.004), whereas positive odors produced a greater synchronization response in the late beta band (around 690 to 780 ms, $t = 3.49$, $P < 0.002$, probability CI range = 0.003) determined by 5,000 Monte Carlo permutation tests.

The separation in processing between the two valence extremes demonstrated that negative odors produced a more pronounced activity in the early beta band. We hypothesized that this early processing might indicate the cuing of an early avoidance response. This would align with behavioral data in humans that have shown that an odor associated with threat elicits a full-body motor avoidance response (10). If this hypothesis is valid, we should observe odor valence-dependent modulation of preparatory motor responses over the motor cortex in the time interval of these OB responses. Specifically, we hypothesized that we would observe greater power in the mu rhythm over the motor cortex for negative odors. Desynchronization in mu rhythm has previously been demonstrated to be a measure of preparatory motor responses to salient stimuli (33, 34), whereas inhibition of motor behavior yields synchronization in mu rhythm (35, 36). To this end, the mu rhythm for two extremes was assessed on the whole scalp, where we found greater power over the motor cortex (electrode C2: $t = 2.17$, $P < 0.014$, probability CI range = 0.003; electrode C4: $t = 3.00$, $P < 0.003$, probability CI range = 0.001; electrode CP2: $t = 2.01$, $P < 0.022$, probability CI range = 0.004; electrode CP4: $t = 3.27$, $P < 0.001$, probability CI range = 0.001; electrode CP6: $t = 2.23$, $P < 0.012$, probability CI range = 0.003).

Iravani et al.
The human olfactory bulb processes odor valence representation and cues motor avoidance behavior

PNAS | 5 of 12
https://doi.org/10.1073/pnas.2101209118

Next, we localized the source of the mu rhythm using extra low-resolution electromagnetic tomography (eLORETA) and found a cluster around the right motor cortex (x 27, y −35, z 60) where the dipole voltage density was 12% stronger for unpleasant compared to pleasant odors. Furthermore, for negative odor trial (defined as 1.5 SD below the group mean), we extracted valence ratings and odor-induced responses and subsequently assessed the effect on mu rhythm for each trial using a generalized linear model with Valence and Intensity as predictors. The group effect of Valence to predict mu power was finally estimated for each electrode using a Student's t test. In line with our hypothesis, negative odor valence was related to mu rhythm power over the motor cortex in the time period of interest (250 to 450 ms after odor onset, the interval was selected slightly larger to increase frequency specificity), electrode CP2: $t(18) = -2.23$, $P < 0.038$, CI $= [-1.39, -0.04]$ and electrode FC4: $t(18) = -2.32$, $P < 0.032$, CI $= [-0.92, -0.046]$ (*SI Appendix*, Fig. S3). In other words, the more negative an odor was perceived, the more mu power over the motor cortex was observed in the time period of the early OB processing.

Unpleasant Odors Elicit a Fast Avoidance Response. Our results so far have suggested that processing in the human OB is attuned to odor valence and that there is a link between processing in the OB and motor cortex activity in a valence-dependent manner. These results suggest an association between valence processing of negative odors in the OB and an early avoidance response. In other words, if the results obtained in Experiment 1 are valid, when a negative odor stimulates the OB, a behavioral avoidance response should be initiated by the motor system in the time period shortly after the demonstrated mu activity, i.e., 400 ms plus motor response time. To directly test this prediction, in Experiment 2, we sought to determine whether odor valence initiates an approach–avoidance response. Specifically, we wanted to determine whether this response is linked in time to the early time period where associations between OB processing and valence perception were found as well as a functional gating was demonstrated between the OB and the motor cortex in the mu band. We operationalized approach–avoidance motor responses as posterior-anterior angular motion, derived from normalized responses from a force plate that measures participants' whole-body microsway (Fig. 4A). We hypothesized that a negative odor would elicit an avoidance response, manifested by the initiation of a backward motion in the early time period of interest. The body microsway was measured as posterior-anterior angular motion that was normalized to the height of individuals and bandpass filtered to produce posterior-anterior momentum (PAM). Two pleasant and two unpleasant odors, with averaged valence ratings illustrated in Fig. 4B, were presented using sniff-triggered olfactometry, identical to what is described for Experiment 1.

We first performed a pilot experiment ($n = 21$) to allow us to determine the time point(s) of interest for analyses of PAM responses in a nonbiased manner, to preregister our hypothesis and analyses, and, importantly, to establish known priors for subsequent Bayesian analyses. To this end, we assessed five time points of interest: 0.25 s (at the time of gamma processing), 0.5 s (the hypothesized period of interest, gamma + response time, based on results in Experiment 1), 0.75 s (at the time of the beta processing), 1.0 s (at the time of beta processing + response time), and 1.25 s after odor onset across the pleasant and unpleasant odor conditions (*SI Appendix*, Fig. S4A). These time points were selected to cover the full odor presentation with additional motor response time factored in. Within a linear mixed effect model (LMM) statistical model, with participant as intercept and conditions as random slope, we found a significant main effect for conditions only at the time point 0.5 s after odor onset, $t(61) = 2.13$, $P < 0.037$, CI =

[0.01, 0.04], with no other significant effects at other time points (*SI Appendix*, Fig. S4B). Subsequent Student's t tests against 0 (standing straight) demonstrated that the backward motion in response to negative odors was significant, $t(61) = 2.06$, $P < 0.04$, CI $= [-0.28, -0.04]$, but without a potential forward motion in response to a positive odor, $t(61) = 0.64$, $P > 0.74$, CI $= [-0.19, 0.39]$.

In the main experiment (Experiment 2; $n = 44$), we focused our analyses on the time point identified in the pilot experiment—all other aspects but the sample size remained identical. We selected the sample size based on an estimated effect size of 0.3 (derived from the pilot experiment) and required power 0.95, alpha error probability 0.05, and a correlation among measures of 0.4—this yields a suggested sample size of 44 participants to enable a strong prediction. All hypothesis and analyses were preregistered at https://aspredicted.org/fk9gw.pdf.

We could replicate the result demonstrated in the pilot experiment with a significant difference between the two odor categories at time point 0.5 s after odor onset, $t(174) = 3.24$, $P < 0.001$, CI $= [0.06, 0.23]$ (Fig. 4C). Given the fact that for Experiment 2 we had a known prior from an independent dataset (result from the pilot experiment), we further explored this effect using Bayesian statistics. The Bayesian analyses supported results obtained with frequentist methods. We found that our analyses gave substantial support for a difference between the two parameters (Bf$_{10}$ = 3.32; *SI Appendix*, Fig. S5). However, these analyses assess potential differences between the two odor categories, whereas results from the pilot experiment indicate that effects are mediated mainly by negative odors. When assessing each odor valence category separately against no movement using a one-sided Student's t test with directionality based on the preregistration, there was once again only a statistically significant effect for the negative odors to elicit a backward motion, $t(174) = 2.47$, $P < 0.007$, CI $= [-\infty, -0.016]$, and no significant effect for the positive odors, $t(174) = 1.22$, $P > 0.11$, CI $= [-0.04, +\infty]$.

We then assessed whether the difference between odor valence in PAM was mediated by a potential difference in respiratory flow, a parameter that previously has been demonstrated to be linked to odor valence (37). However, we found no correlation between the respiration flow and PAM at the time point of interest (0.5 s), $rho = -0.02$, $P > 0.75$, (Fig. 4D). Moreover, to verify the lack of dependency, we assessed the null effect using Bayesian statistics with the known priors. These analyses also supported the conclusion that PAM and respiration were not interdependent (*SI Appendix*, Fig. S6).

Discussion

We here demonstrate that neural activity in the human OB is linked to perceived odor valence. Specifically, we found that the OB processes odor information sequentially within two time periods: First, a brief period of initial gamma activity across the valence dimension and a temporally privileged early beta activity for unpleasant odors, both indirectly linked to the cuing of a motor avoidance response. Second, there was a later period of beta processing that was linked to the linear formation of the final subjective valence percept of the presented odor. These results indicate that one of the initial and primary functions of the OB is to process early odor-based valence information, potentially to extract early odor-based warning signals.

The observation that odor valence was processed in the human OB mainly during two time points, one early and one late stage, is in line with the two-stage model of odor processing in the OB suggested by Frederic et al. (38). They specifically demonstrated that the OB first executes a fast processing, relying on gamma oscillations, allowing the individual to make fast
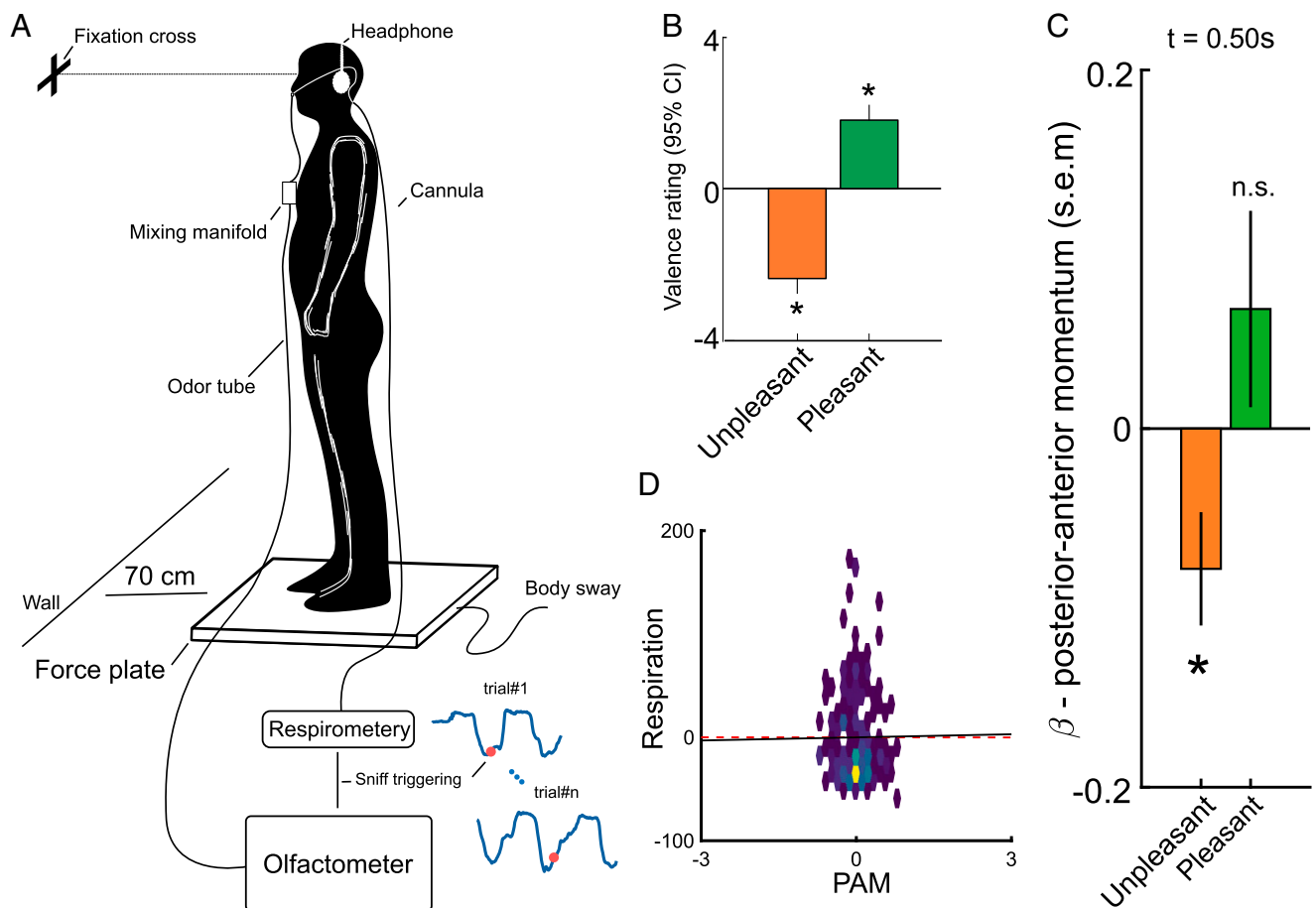
Iravani et al.
The human olfactory bulb processes odor valence representation and
cues motor avoidance behavior

Fig. 4. Unpleasant odors elicit a fast avoidance response. (*A*) Experimental setup in pilot and Experiment 2. Participants stood centrally on the force plate with their feet together, facing a wall with a fixation cross placed at their eye level. Continuous respiration was measured using a respirometer, and the olfactometer was triggered close to the nadir of a respiration cycle to synchronize the trial onset with inhalation. (*B*) Bars show averaged valence rating of unpleasant and pleasant odors during the experiment (error bars show 95% CI). (*C*) Valence-dependent modulation of PAM was replicated in the main experiment in line with our preregistered hypothesis and indicating significant backward movement (i.e., beta values below zero) for unpleasant odors 500 ms after odor onset. (*D*) Nonsignificant correlation coefficient between PAM and respiration flow suggest that differences in breathing did not facilitate differences. Heatmap shows the joint distribution, and the dashed red line shows the correlation. *$P < 0.05$.

discriminations, and a second slower processing, relying on beta oscillations, utilizing information from centrifugal inputs to support more deliberate decisions. Our data, which is in line with earlier human and animal work, suggests that the OB processes valence of unpleasant and pleasant odors at different time points. In this context, our link between early gamma and beta (for unpleasant odors) oscillations in the OB suggests that this might be a preparatory, nondeliberate mechanism for fast avoidance of potentially dangerous odors or avoidance of their sources. This hypothesis is further supported by previous findings that odor-induced gamma oscillations within the OB are largely a local phenomenon (39, 40) and sometimes dependent on the individual's behavioral state or past negative experience with the odor (41). Moreover, because the OB is located very early in the odor processing stream with projections from the olfactory receptor neurons and monosynaptic connections to cerebral areas associated with processing of information related to threat/saliency (42), the OB is ideally localized in the processing pipeline to process avoidance-related information given the need for a fast response. Indeed, associating an odor with an aversive outcome alters a range of parameters in how the OB processes the associated odor. For example, it increases neural responses (1, 43) as well as axonal density into associated glomeruli, which in turn is associated with an increase in associated glomeruli size (44). Based on our past findings, it is

therefore likely that one of the initial and important aspects of the OB is to extract and process odor information that is associated with a potential threat.

Results from the modularity index, derived from the PC analyses, indicated that the strongest link between the two time periods and final odor valence rating was the later beta activity occurring around 700 to 800 ms after odor onset. This is also in line with the two-stage model (38) of odor processing in the OB with a separation of processing between bottom-up and top-down dependent processing. Beta oscillations are often considered more of a "top-down"–dependent signal as opposed to gamma oscillations, which are considered more of a "bottom-up"–dependent signal (45–47), although it should be made clear that beta has also been demonstrated to be initiated in the OB during odor sampling (48). Past studies in animal models have indeed linked gamma band processing within the OB to intrabulb processing (39, 47), and beta processing has been demonstrated to sometimes be dependent on centrifugal feedback from piriform cortex (49, 50) and to be modulated by context or past odor associations (38). Our data cannot, however, conclusively determine whether the OB activity in the later time period originates from centrifugal information from higher order areas. Nonetheless, we believe that the most parsimonious explanation is that the late beta is representing valence-dependent signals that project back, directly or

Iravani et al.
The human olfactory bulb processes odor valence representation and
cues motor avoidance behavior

PNAS | 7 of 12
https://doi.org/10.1073/pnas.2101209118

indirectly, from other cerebral areas, such as the orbitofrontal, amygdala, and piriform cortex. These projections would then help shape the final interpretation of the odor by adding information of past experiences (51) as well as information about the odor object per se (52–54)—two factors that are known to strongly influence the final odor valence percept (4, 55). Nonetheless, the analysis we performed in this study was unable to demonstrate directionality and future studies need to determine this specific question.

In our data, the early gamma and beta power in the OB seem specifically attuned to the processing and perception of negative odor valence with no clear demonstration that the OB processes odors associated with a positive outcome at early time points. This finding is in line with findings in rodents indicating that the anterior OB is processing negative or aversive odors, whereas odors with a positive valence are processed mainly within an area downstream from the OB, the olfactory tubercle (56, 57), an area that does not have centrifugal direct connections with the OB (58). Whether this region-specific valence separation in processing also occurs in humans is not known. However, a recent study on human participants demonstrated that, akin to rodents, pleasant but not negative odors are preferentially processed in the olfactory tubercle (59). Moreover, intracranial electric stimulation of the OFC, an area previously linked to odor valence processing in humans, could only produce pleasant odor experiences (60). This separation between valence extremes support the 2D valence hypothesis postulating that odor valence perception is not represented by a unidimensional spectrum, ranging from unpleasant to pleasant. Instead, a 2D space where positive and negative valence is separated with neutral valence as the start point has been suggested (32). This has also been supported by data on the semantic distribution of odor descriptors that are commonly divided into a positive and a negative category (32, 61). In contrast to the demonstrated increase in beta frequency for odors with more negative valence as compared to odors with more positive valence, we did not find an association between valence and beta activity when assessing links in RSA space using a linear approach in early time points. A possible explanation for this discrepancy might be that our t-PAC finding suggests that the detailed odor valence information for beta is reflected in phase and not amplitude in early time periods of OB processing of the odor. Hence, it is possible that the lack of linear association between neural activity in beta band and odor valence in RSA space during early time points is due to our finding that only phase, but not amplitude, based on PAC coupling, is linked to gamma, thereby suggesting that the coupling of amplitude is critical for finding linear associations in RSA space. Similarly, our present method may not be able to capture that the OB also processes positive valence during early time points due to the range of our odors used where only some mean individual ratings reached above 70 on the 0 to 100 scale (Fig. 1B).

When studying OB function, a confounding factor is the possible effect of respiration change, modulated by odor valence. Past studies demonstrate that unpleasant odors can modulate the sniff magnitude (62), which in turn affects OB activity (63). Hence, a negative odor can indirectly change OB activity by mere modulation of respiration and not directly through receptors. That said, both animal (64) and intracranial recordings in humans (65) demonstrate that respiration mainly affects slower frequencies in the theta/delta bands in the brain. When considering the fact that oscillations in the present data (i.e., gamma/ beta) are well separated from theta/delta bands and that no changes were found in breathing parameters between odors (*SI Appendix*, Fig. S3), it is unlikely that our findings are significantly affected by potential differences in respiration. It should further be noted that the EBG method requires that participants are in a nutrition-deprived state to maximize signals from

the OB, which might have an impact on the obtained results (9, 66, 67). However, this later aspect of the method can also mean that the potential perceived reward of the cue odor would increase and therefore also maximizes the likelihood of finding effects for positive odors. Future studies where odors are either individually selected based on their reward properties or conditioned with positive outcome are needed to conclusively determine whether the human OB prioritizes processing negative odor valence.

Results in Experiment 1 suggested the existence of an approach/avoidance motor response occurring around 500 ms after odor onset in a valence-dependent manner. In two separate experiments (pilot and Experiment 2) and using a design with preregistered hypotheses and analyses, we demonstrate here that odors with a negative valence triggered an avoidance response that was manifested as leaning away from the odor source. We have previously demonstrated a similar fast avoidance response in human participants to the odor of blood (10), an odor that is treated as an approach or avoidance trigger across species. Our current findings extend these results and suggest that odor avoidance in humans might extend beyond biologically important and potentially inherent signals and be a general phenomenon that is linked to the valence of the odor per se. Negative odors induced larger mu desynchronization over and within the motor cortex, which is a response that previously has been demonstrated to be a measure of preparatory motor responses to salient stimuli (33, 34). Although speculative, this mu desynchronization appeared in a time period that, when response time is factored in, corresponds to the motor avoidance response to negative odors demonstrated in Experiment 2. Moreover, this motor cortex response to the negative odors appeared around 150 ms after the valence-related increase in gamma and early beta activity within the OB, thereby allowing the signal time needed to transmit the information between the OB and motor cortex. For neutral and pleasant odors, a similar motor movement would probably be related to later processing. In line with this notion, rodents performing a Go, No-Go task with positive reinforcement exhibit simultaneous activity in the piriform cortex and primary motor cortex just before executing a motor response for the Go trials. Importantly, while these responses are seen in low and high gamma, as well as beta activity, they are only present during the second and the third and final sniff (68). For the first sniff (equivalent to the data in our study), there was, however, no response related to the motor cortex for the rewarded Go trials. This indicates that for neutral and pleasant odors, as compared to unpleasant, a top-down regulation from olfactory cortex and motor cortex directly to the OB is more evident (68). Our results suggest that the olfactory and motor systems are also more closely linked in humans than has previously been appreciated and that this, especially for unpleasant odors, may be cued at the OB level.

It should be noted that while our results demonstrate that the human OB processes subjective odor valence, it does not suggest that the OB is the first processing stage of valence. Multiple studies in humans and nonhuman animals alike show that an odorant's valence partially depends on its physicochemical properties (69–75). Physicochemical properties have been shown to predict olfactory receptor neuron activation, and based on this, it has been suggested that odor valence is, at least partially, coded at the level of the olfactory epithelium (74). Because the six odors in Experiment 1 were selected from the DREAM challenge (75) to span the physicochemical valence space, our OB activations may to some extent reflect information from physicochemical properties originating from receptor neurons projecting upstream to the OB (76). It is still an open question if a peripheral valence code originating from physicochemical properties reaches the OB and if the OB in

turn refines the signal or keeps it unchanged. It should, however, be noted that all results linking odor valence to OB processing are based on the individual's own valence rating and not an a priori defined valence rank among the included odors. Specifically, we show that perceived pleasantness is represented uniformly across participants in the bulb at specific time periods and frequencies in a manner that is represented by subjective perception and not predefined odor classification. This suggests that valence is processed and not merely manifested by odor identity. Valence ratings are, to a nontrivial degree, dependent on personal experiences. Indeed, when we assess the relationship between individual's RDM of odor valence ratings and that of the full group, the mean similarity is 61.6%, which means that about 38.2% of the total variance in these valence ratings (in this case, valence ranking) is explained by individual differences. Our choice of methods therefore reduces, but does not eliminate, the potential impact physicochemical properties might have on our results in favor of subjective valence perception.

Even though we can demonstrate links between the OB and the motor cortex in a relevant time period, it should be noted that our whole-body avoidance results are only indirectly linked to the EEG data. For it to be directly linked, it would require assessing EEG source signals from individuals who are freely moving around, which is not possible with current methods for measuring OB responses because the active electrodes strongly amplify motion artifacts. To the best of our knowledge, no method currently exists that would allow measures from the OB while participants moved their full body. Moreover, it is important to highlight that our data only covers the first sniff of an unannounced odor. As demonstrated in rodents, OB processing is continuously updated with each continuous sniff with marked shifts in both neural and behavioral responses (68, 77, 78).

In summary, our results suggest that the human OB processes odor valence. We propose that the two stages of processing of valence in the OB are due to a reciprocal process where the initial fast gamma and beta response address negative odors based on valence information that may be projected from the olfactory receptor neurons (69) or learned from past aversive experiences already coded in the OB (1). In contrast, the later beta response seems more related to the final valence rating of the odor as well as potential preparation of the OB's initial gamma and subsequent beta responses for the second sniff of the same odor. At this stage, the OB should be influenced by information related to past experiences with the identity of the odor. Importantly, negative odors seem to have privileged temporal access in the human OB. This suggests that one of the initial functions of the OB is to process and extract early odor-based warning signals to aid the individual's approach–avoidance decisions.

Methods

Experiment 1: Valence Decoding from Oscillations within the OB.

Participants. In Experiment 1, 19 individuals (mean age 28.88 ± 4.52, 7 women) who reported being healthy, nonsmokers, and with no history of head trauma or neurological disorders participated in three separate recording sessions (all identical). Prior to inclusion, a working sense of smell was confirmed in all participants using a five item, four alternative, cued odor identification test (79). All participants cleared the cutoff for inclusion of at least three correct answers. Given the scarcity of functional anosmia in the participants' age range, the probability that we erroneously included individuals with anosmia in the experiment is less than 0.05%. The study was approved by the national Swedish Ethical Review Authority (EPN: 2016/1692-31/4), and all participants signed informed consent prior to participation.

Chemicals and odor delivery. In Experiment 1, six odorants were used, namely linalool, ethyl butyrate, 2-phenyl-ethanol, 1-oceten-3-ol, octanoic acid, and diethyl disulfide (*SI Appendix*). Odors were delivered birhinally using a computer-controlled olfactometer (11), and each odor was presented 20 times in each session to participants (i.e., 60 times in total for each odor across the three sessions). The olfactometer has an onset time of 200 ms, measured

from computer trigger to odor delivered in the nose, and a sharp rise time to facilitate an odor presentation with high temporal precision (11). A total flow rate of 3 L/min inserted into a constant 0.3 L/min flow to prevent tactile sensation of odor onset was used. To further avoid participants predicting odor onset but ensure a clear percept, odor onset was (unbeknownst to the participants) triggered by their own sniff cycle. When the assigned intertrial interval (10 s) had occurred, an odor was triggered at the nadir of the inhalation phase in the sniff cycle following that interval, thus ensuring odor presentation at inhalation. A relatively long intertrial interval was used to lower the risk of odor habituation. Participants' sniff cycle was measured by thermopod (Experiment 1) and respirometer (Experiment 2) sampling at a rate of 400 Hz (Powerlab 16/35, ADInstruments), and respiration traces for triggering of odor were analyzed online by LabChart recording software (ADInstrument). Data were subsequently down-sampled offline to 40 Hz and processed in MATLAB 2018a for further analyses.

Procedure. To allow us to collect a large data set for each individual, each participant participated in three sessions on separate days with at least 1 d and at the most 1 mo apart. Each session consisted of three 15-min long blocks with 5-min break between each to limit odor adaptation/habituation, totaling about 1 h per session. Participants were presented with the six different odors in a random order and after each odor presentation, they rated how pleasant and intense they perceived the presented odor to be. Ratings were done by placing a marker on a labeled visual analog scale presented on the screen ranging from 0 (very unpleasant/very weak) to 100 (very pleasant/very strong).

Electroencephalography, EBG, neuronavigation measurement. Sixty-four EEG scalp electrodes were placed according to international 10/20 standard and an additional four EBG electrodes on the forehead (9). Signals were sampled at 512 Hz using active electrodes (ActiveTwo, Bio-Semi) and the recording from both 64 EEG and 4 EBG electrodes was used to interpolate surface potentials on scalp as well as forehead. Subsequently, these recordings were used to reconstruct OB time course on the source level. Electrode offsets were manually checked prior to experiment onset, and electrodes were adjusted until meeting the a priori established criteria (<40 mV). Next, the position of all the electrodes in stereotactic space was determined using an optical neuronavigation system (Brain-Sight, Rogue Research); for more details, please see ref. 9.

EBG/EEG data analysis. Preprocessing. Data were epoched from 500 ms prestimulus to 1,500 ms poststimulus, rereferenced to average of activity at all electrodes, linear phase bandpass filtered at 1 to 100 Hz (Butterworths fourth order), and power-line interference filtered using discrete Fourier transform filtering at electrical frequency (50 Hz) to remove power-line noise. Trials with large muscle and eye blink artifacts were identified with an automatic algorithm. The artifact detection protocol consisted of bandpass filtering using Butterworth filter (fourth order), Hilbert transform to extract amplitude values, and z-scoring. Trials with z-values above 4 were marked and removed from further analysis.

OB time course extraction. To extract OB's response time course, digitized electrode positions were first used to coregister the participant's head to a default Montreal Neurological Institute (MNI) brain using a six-parameter affine transformation. Second, a head model was constructed based on a multishell spherical head model. Spherical volume conductors were considered for scalp, skull, gray matter, and white matter with the conductivity of 0.43, 0.01, 0.33, and 0.14 (9). The covariance matrix of 64 scalp and 4 EBG electrodes during the 1 s odor presentation were regularized by 10% prior to being fed into eLORETA algorithm to estimate the time course of the dipole placed in ($x \pm 6$, y 30, z −32) on trial level, which corresponds to OB location (9, 80). The maximum projection of the dipoles' time course over three principal axes was computed to serve as OB activity. eLORETA analysis was carried out in the open-source Fieldtrip toolbox 2018 within MATLAB R2019b (81).

Time-frequency analysis of OB signal. After extracting the OB's response time course, we assessed the difference in power evolution of the two most unpleasant and pleasant odors. The time-frequency map for broadband frequencies [1~100 Hz], with step of 1 Hz and interval [−0.1~1 s] with step of 0.005 s, was estimated using a multitapered sliding window from discrete prolate spheroidal sequences (DPSS). The window length was adjusted to cover at least three cycles for each frequency, ranging 0.3~3 s. Next, the time-frequency map of each trial was assessed and converted to decibels. Finally, to create the contrast map, the most unpleasant and pleasant category, each consisting of two odors, was determined on the individual level based on participants' valence ratings and contrasted against each other.

Mu rhythm and source localization. Similar to time-frequency analysis of OB signal, the mu rhythm power for all scalp electrodes were estimated using

Iravani et al.
The human olfactory bulb processes odor valence representation and
cues motor avoidance behavior

PNAS | 9 of 12
https://doi.org/10.1073/pnas.2101209118

multitapered sliding DPSS widow for mu frequency range [10~13 Hz] with step of 0.5 Hz and time interval of 0.3~0.4 s with step of 0.005 s. Likewise to OB time-frequency analysis, the window lengths were chosen to cover at least three cycles of mu rhythm. Next, the mu power for the two most unpleasant and pleasant odors were estimated, baseline corrected, and converted to decibels. Finally, a topographical map was created and nonparametric statistics were performed to create contrast and find channels that were significantly different in mu power. Source localization was performed similar to the OB source localization, and after coregistration of electrodes to default MNI brain, a spherical head model with four tissue types was created. The cross-spectral density matrix of electrodes during the 0.3~0.4 s after the odor onset were regularized by 10% and fed into eLORETA to localize the source of mu rhythm.

t-PAC. t-PAC of the extracted OB response time course was analyzed between gamma and beta bands with window length 250 ms and 50% overlapping. The gamma band [30~100 Hz], discretized to 20 frequency bins, and the instantons amplitude were extracted using Hilbert transform at each frequency bin. Similarly, using Hilbert transformation , the instantaneous phase of slower oscillations (i.e., beta [12~30 Hz]) was computed, and t-PAC for each time bin was calculated as the power ratio of the composite signal of instantaneous amplitude of faster oscillation and phase of slower to the faster oscillation during the window interval on the individual level (25). Moreover, we quantified the comodulogram level between the outcome of t-PAC with a slower band to isolate a range of slower frequencies that are coupled to identified gamma. t-PAC analysis were carried out in BrainStorm toolbox within MATLAB R2019b (82).

RSA. We used RSA to assess the relationship between the odor valence rating and neuronal population activity of OB in two prominent odor-related frequencies, gamma and beta. To limit our statistical tests and minimize the potential false positive error, we only include the frequencies of gamma and beta bands in the RSA analysis that were found to be coupled in the t-PAC analysis. The RDMs for whole 1 s of odor stimuli were compared between the behavioral and OB response in a searchlight framework on the individual level. In line with a multidimensional scaling method (14), the so-called DISTATIS method, we constructed a consensus RDM to represent the group level. To determine the potential relationship between neural and perceptual RDMs, values above the diagonal line of the matrices was assessed using all possible permuted (i.e., shuffling the labels of odors; given 6 odors, the total possible combinations is 720) partial Pearson correlation to avoid inflated correlation due to symmetry of RDMs (Fig. 1*A*). The group-level RDMs were subsequently scaled down using eigenvector decomposition into two main axes. The distance matrices were converted to similarity matrices by inversing the distance matrix after added by 1, and modularity indices (Q) were computed using the Newman method (30) given three clusters. The three clusters were identified using a hierarchical clustering of valence rating, varying the number of clusters from 1 to 6 and estimating the knee of the modularity curve where the knee of the curve was estimated as the furthest point from the linear approximation. RSA analysis and community detection were performed in the open-source CoSMoSMVPA toolbox (83) and MATLAB Network Toolbox (https:// github.com/ivanbrugere/matlab-networks-toolbox).

Statistical analysis. We assessed the statistical difference in power evolution between the two most unpleasant and pleasant odors, as well as scalp mu rhythm, using a nonparametric statistic. The time-frequency maps of unpleasant and pleasant odors of OB signal and scalp electrodes were computed using multitapered sliding windows and compared using 5,000-permutation Monte Carlo tests to find significance time/frequency bins or channels. To statically test the relationship between the brain data and valence rating in RSA, RDM matrices at each time point were shuffled through all possible combinations. In each iteration, partial Pearson correlation between neural and perceptual valence was computed with intensity as nuisance covariates. To extract the exact *P* value from the permutation test, we computed the number of times the actual partial Pearson correlation was bigger than shuffle data out of total permutations (720). Similarly, for t-PAC analysis, nonparametric Monte Carlo 5,000 permutation tests were performed for the OB coupling value at each time-frequency bin against baseline (250 ms prestimulus), and exact *P* value were extracted. The subsequent t-map was smoothed, while preserving the shape, for illustration purposes.

The distance matrices at the instances of significant correlation with valence for both gamma and beta were scaled down to first and second PCs (i.e., PC1 and PC2), and Newman modularity was calculated to assess whether the tested odors clusters comply with valence rating. To statistically test the Newman index Q, the modularity of similarity matrices was compared with the null model for each correlation peak. The null model was generated by 5,000 times rewiring of the adjacency (similarity) matrix while persevering weight, degree, and strength distribution using the Brain Connectivity Toolbox within MATLAB R2019b (84, 85). Later, the actual modularity index was compared with the null distribution. In the post hoc analysis to assess effects on premotor responses, we extracted data in the time interval 300 to 400 ms after odor onset. We tested if the preparatory response for motor action we observed in Experiment 2 could be found in this experiment, even though here, participants were sitting in a chair and instructed to sit as still as possible. The power of mu synchronization/desynchronization was predicted using a generalized linear model having valence and intensity as predictors for each electrode on the scalp and yielding in beta maps on the individual level. Subsequently, the beta maps were statically tested on the group level via the Student's *t* test.

Experiment 2: Odor Valence–Dependent Approach/Avoidance Responses.
Participants. Given that links between perceived odor valence and approach/ avoidance motor responses had not been previously assessed, we initially performed a structured pilot experiment to explore the time period of interest of the motor response, the result of which was later used as a priori defined temporal regions of interest in Experiment 2. In the pilot experiment, a total of 21 individuals (age = 28.71 ± 5.84, 11 women) participated. In the subsequent Experiment 2, a total of 44 individuals (age = 25.52 ± 4.01, 26 women) participated. Inclusion criteria (including passing the anosmia screening test) were the same as described for Experiment 1. The studies were approved by the local ethical review board (EPN: 2016/1692-31/4), and all participants signed informed consent prior to their participation.

Odors and delivery method. In both the pilot and main experiments, odors were piloted and presented as described in Experiment 1 but using slightly different odors. In the pilot experiment, four odors were used, namely strawberry, carvone, fish odor, and ethanethiol. To limit odor dependency, strawberry was substituted with vanillin and ethanethiol with diethyl disulfide in the main experiment (*SI Appendix*). Odors were presented identical to Experiment 1 and, unbeknownst to the participants, triggered by their sniff cycle (Fig. 4*A*).

Body sway measurement. Participant's body microsway was assessed with a force plate (AccSway^Plus, AMTI Massachusetts) assessing eight axes of motion. The force plate was initially allowed to warm up for a few minutes, after which it was zeroed, and a 25-s period of unloaded baseline was initially recorded for calibration purposes.

Procedure. Participants stood in the center of the force plate with their feet together, facing a wall where a fixation cross was placed at eye height about 70 cm away from their face. The height of the fixation cross was adjusted for each individual according to the participant's height. Their arms were positioned alongside the body, and they were instructed to avoid performing redundant movement (Fig. 4*A*). See *SI Appendix* for more information.

Statistical analyses. Posterior-anterior angular momentum extracted from the body sway data recorded by the force plate was assessed according to a calibration matrix provided by the force plate vendor. In the pilot study (*n* = 21), event-related responses of the PAM were calculated for five time points during the odor interval with steps of 0.25 s to identify the time point of interest. LMM with participant intercept and random slope of odor were fitted for the three time points. Having determined the time point of interest, we repeated the experiment in a completely new data set with bigger sample size and fitted LMM with the exact similar design. Moreover, as a control analysis, we examined if respiration correlates PAM by means of Pearson correlation at the time point of interest. The analysis was repeated in a Bayesian framework as supplementary analysis. See *SI Appendix* for more information.

Data Availability. EEG and behavioral data as well as all scripts have been deposited in the Open Science Framework (https://osf.io/c8u39/?view_ only=ebb85532e1064d128db79bacb6be27f8).

1. L. M. Kay, G. Laurent, Odor- and context-dependent modulation of mitral cell activity in behaving rats. *Nat. Neurosci.* **2**, 1003–1009 (1999).

2. K. Kobayakawa *et al.*, Innate versus learned odour processing in the mouse olfactory bulb. *Nature* **450**, 503–508 (2007).

10 of 12 | **PNAS**
https://doi.org/10.1073/pnas.2101209118

Iravani et al.
The human olfactory bulb processes odor valence representation and cues motor avoidance behavior

3. M. G. Haselton, D. Nettle, The paranoid optimist: An integrative evolutionary model of cognitive biases. *Pers. Soc. Psychol. Rev.* **10**, 47–66 (2006).

4. Y. Yeshurun, N. Sobel, An odor is not worth a thousand words: From multidimensional odors to unidimensional odor objects. *Annu. Rev. Psychol.* **61**, 219–241 (2010).

5. J. Seubert, C. Regenbogen, U. Habel, J. N. Lundström, "Behavioral and neural determinants of odor valence perception" in *Springer Handbook of Odor*, A. Buettner, Ed. (Springer, 2017), pp. 99–100.

6. J. D. Mainland, J. N. Lundström, J. Reisert, G. Lowe, From molecule to mind: An integrative perspective on odor intensity. *Trends Neurosci.* **37**, 443–454 (2014).

7. W. Doucette *et al.*, Associative cortex features in the first olfactory brain relay station. *Neuron* **69**, 1176–1187 (2011).

8. F. Kermen *et al.*, Topographical representation of odor hedonics in the olfactory bulb. *Nat. Neurosci.* **19**, 876–878 (2016).

9. B. Iravani, A. Arshamian, K. Ohla, D. A. Wilson, J. N. Lundström, Non-invasive recording from the human olfactory bulb. *Nat. Commun.* **11**, 648 (2020).

10. A. Arshamian *et al.*, A mammalian blood odor component serves as an approach-avoidance cue across phylum border - from flies to humans. *Sci. Rep.* **7**, 13635 (2017).

11. J. N. Lundström, A. R. Gordon, E. C. Alden, S. Boesveldt, J. Albrecht, Methods for building an inexpensive computer-controlled olfactometer for temporally-precise experiments. *Int. J. Psychophysiol.* **78**, 179–189 (2010).

12. K. Ohla, J. N. Lundström, Sex differences in chemosensation: Sensory or emotional? *Front. Hum. Neurosci.* **7**, 607 (2013).

13. N. Kriegeskorte, M. Mur, P. Bandettini, Representational similarity analysis - connecting the branches of systems neuroscience. *Front. Syst. Neurosci.* **2**, 4 (2008).

14. H. Abdi, A. J. O'Toole, D. Valentin, B. Edelman, "DISTATIS: The analysis of multiple distance matrices" in *2005 IEEE Computer Society Conference on Computer Vision and Pattern Recognition (CVPR'05) - Workshops* (IEEE, 2005), p. 42.

15. G. Buzsáki *et al.*, Hippocampal network patterns of activity in the mouse. *Neuroscience* **116**, 201–211 (2003).

16. A. Bragin *et al.*, Gamma (40-100 Hz) oscillation in the hippocampus of the behaving rat. *J. Neurosci.* **15**, 47–60 (1995).

17. K. Kendrick *et al.*, Learning alters theta-nested gamma oscillations in inferotemporal cortex. *Nat. Prec.*, 10.1038/npre.2009.3151.2 (2009).

18. P. Lakatos *et al.*, An oscillatory hierarchy controlling neuronal excitability and stimulus processing in the auditory cortex. *J. Neurophysiol.* **94**, 1904–1911 (2005).

19. N. Axmacher *et al.*, Cross-frequency coupling supports multi-item working memory in the human hippocampus. *Proc. Natl. Acad. Sci. U.S.A.* **107**, 3228–3233 (2010).

20. M. X. Cohen *et al.*, Good vibrations: Cross-frequency coupling in the human nucleus accumbens during reward processing. *J. Cogn. Neurosci.* **21**, 875–889 (2009).

21. B. Händel, T. Haarmeier, Cross-frequency coupling of brain oscillations indicates the success in visual motion discrimination. *Neuroimage* **45**, 1040–1046 (2009).

22. A. B. L. Tort, R. W. Komorowski, J. R. Manns, N. J. Kopell, H. Eichenbaum, Theta-gamma coupling increases during the learning of item-context associations. *Proc. Natl. Acad. Sci. U.S.A.* **106**, 20942–20947 (2009).

23. C. E. Schroeder, P. Lakatos, Low-frequency neuronal oscillations as instruments of sensory selection. *Trends Neurosci.* **32**, 9–18 (2009).

24. J. Losacco, D. Ramirez-Gordillo, J. Gilmer, D. Restrepo, Learning improves decoding of odor identity with phase-referenced oscillations in the olfactory bulb. *eLife* **9**, e52583 (2020).

25. S. Samiee, S. Baillet, Time-resolved phase-amplitude coupling in neural oscillations. *Neuroimage* **159**, 270–279 (2017).

26. B. N. Johnson, J. D. Mainland, N. Sobel, Rapid olfactory processing implicates subcortical control of an olfactomotor system. *J. Neurophysiol.* **90**, 1084–1094 (2003).

27. J. Prescott, J. Burns, R. A. Frank, Influence of odor hedonics, food-relatedness, and motivational state on human sniffing. *Chemosens. Percept.* **3**, 85–90 (2010).

28. D. G. Laing, Natural sniffing gives optimum odour perception for humans. *Perception* **12**, 99–117 (1983).

29. H. Manabe, K. Mori, Sniff rhythm-paced fast and slow gamma-oscillations in the olfactory bulb: Relation to tufted and mitral cells and behavioral states. *J. Neurophysiol.* **110**, 1593–1599 (2013).

30. M. E. J. Newman, M. Girvan, Finding and evaluating community structure in networks. *Phys. Rev. E Stat. Nonlin. Soft Matter Phys.* **69**, 026113 (2004).

31. S. Maslov, K. Sneppen, Specificity and stability in topology of protein networks. *Science* **296**, 910–913 (2002).

32. S. S. Schiffman, Physicochemical correlates of olfactory quality. *Science* **185**, 112–117 (1974).

33. S. Kumar, M. J. Riddoch, G. Humphreys, Mu rhythm desynchronization reveals motoric influences of hand action on object recognition. *Front. Hum. Neurosci.* **7**, 66 (2013).

34. J. Matsumoto *et al.*, Modulation of mu rhythm desynchronization during motor imagery by transcranial direct current stimulation. *J. Neuroeng. Rehabil.* **7**, 27 (2010).

35. R. C. Howe, M. B. Sterman, Cortical-subcortical EEG correlates of suppressed motor behavior during sleep and waking in the cat. *Electroencephalogr. Clin. Neurophysiol.* **32**, 681–695 (1972).

36. G. Pfurtscheller, C. Brunner, A. Schlögl, F. H. Lopes da Silva, Mu rhythm (de)synchronization and EEG single-trial classification of different motor imagery tasks. *Neuroimage* **31**, 153–159 (2006).

37. R. A. Frank, M. F. Dulay, R. C. Gesteland, Assessment of the Sniff Magnitude Test as a clinical test of olfactory function. *Physiol. Behav.* **78**, 195–204 (2003).

38. D. E. Frederick *et al.*, Gamma and beta oscillations define a sequence of neurocognitive modes present in odor processing. *J. Neurosci.* **36**, 7750–7767 (2016).

39. C. Martin, N. Ravel, Beta and gamma oscillatory activities associated with olfactory memory tasks: Different rhythms for different functional networks? *Front. Behav. Neurosci.* **8**, 218 (2014).

40. C. M. Gray, J. E. Skinner, Centrifugal regulation of neuronal activity in the olfactory bulb of the waking rabbit as revealed by reversible cryogenic blockade. *Exp. Brain Res.* **69**, 378–386 (1988).

41. L. M. Kay, Two species of gamma oscillations in the olfactory bulb: Dependence on behavioral state and synaptic interactions. *J. Integr. Neurosci.* **2**, 31–44 (2003).

42. J. Mainland, N. Sobel, The sniff is part of the olfactory percept. *Chem. Senses* **31**, 181–196 (2006).

43. M. L. Fletcher, Olfactory aversive conditioning alters olfactory bulb mitral/tufted cell glomerular odor responses. *Front. Syst. Neurosci.* **6**, 16 (2012).

44. S. V. Jones, D. C. Choi, M. Davis, K. J. Ressler, Learning-dependent structural plasticity in the adult olfactory pathway. *J. Neurosci.* **28**, 13106–13111 (2008).

45. A. Gnaedinger, H. Gurden, B. Gourévitch, C. Martin, Multisensory learning between odor and sound enhances beta oscillations. *Sci. Rep.* **9**, 11236 (2019).

46. C. G. Richter, W. H. Thompson, C. A. Bosman, P. Fries, Top-down beta enhances bottom-up gamma. *J. Neurosci.* **37**, 6698–6711 (2017).

47. L. M. Kay, Circuit oscillations in odor perception and memory. *Prog. Brain Res.* **208**, 223–251 (2014).

48. B. Gourévitch, L. M. Kay, C. Martin, Directional coupling from the olfactory bulb to the hippocampus during a go/no-go odor discrimination task. *J. Neurophysiol.* **103**, 2633–2641 (2010).

49. S. L. Bressler, Spatial organization of EEGs from olfactory bulb and cortex. *Electroencephalogr. Clin. Neurophysiol.* **57**, 270–276 (1984).

50. C. Martin, R. Gervais, B. Messaoudi, N. Ravel, Learning-induced oscillatory activities correlated to odour recognition: A network activity. *Eur. J. Neurosci.* **23**, 1801–1810 (2006).

51. W. Li, J. D. Howard, T. B. Parrish, J. A. Gottfried, Aversive learning enhances perceptual and cortical discrimination of indiscriminable odor cues. *Science* **319**, 1842–1845 (2008).

52. D. A. Wilson, R. M. Sullivan, Cortical processing of odor objects. *Neuron* **72**, 506–519 (2011).

53. D. K. Porada, C. Regenbogen, J. Seubert, J. Freiherr, J. N. Lundström, Multisensory enhancement of odor object processing in primary olfactory cortex. *Neuroscience* **418**, 254–265 (2019).

54. J. K. Olofsson *et al.*, A designated odor-language integration system in the human brain. *J. Neurosci.* **34**, 14864–14873 (2014).

55. J. Djordjevic *et al.*, A rose by any other name: Would it smell as sweet? *J. Neurophysiol.* **99**, 386–393 (2008).

56. M. A. Gadziola, K. A. Tylicki, D. L. Christian, D. W. Wesson, The olfactory tubercle encodes odor valence in behaving mice. *J. Neurosci.* **35**, 4515–4527 (2015).

57. M. A. Gadziola, D. W. Wesson, The neural representation of goal-directed actions and outcomes in the ventral striatum's olfactory tubercle. *J. Neurosci.* **36**, 548–560 (2016).

58. E. E. in 't Zandt, H. L. Cansler, H. B. Denson, D. W. Wesson, Centrifugal innervation of the olfactory bulb: A reappraisal. *eNeuro*, 10.1523/ENEURO.0390-18.2019 (2019).

59. M. Midroit *et al.*, Neural processing of the reward value of pleasant odorants. *Curr. Biol.* **31**, 1592–1605.e9 (2021).

60. N. Bérard *et al.*, Electrical stimulation of the medial orbitofrontal cortex in humans elicits pleasant olfactory perceptions. *Epilepsy Behav.* **114**, 107559 (2020).

61. S. Schiffman, D. E. Robinson, R. P. Erickson, Multidimensional scaling of odorants: Examination of psychological and physicochemical dimensions. *Chem. Senses* **2**, 375–390 (1977).

62. P. Joussain, M. Thevenet, C. Rouby, M. Bensafi, Effect of aging on hedonic appreciation of pleasant and unpleasant odors. *PLoS One* **8**, e61376 (2013).

63. A. H. Moberly *et al.*, Olfactory inputs modulate respiration-related rhythmic activity in the prefrontal cortex and freezing behavior. *Nat. Commun.* **9**, 1528 (2018).

64. L. M. Kay, Theta oscillations and sensorimotor performance. *Proc. Natl. Acad. Sci. U.S.A.* **102**, 3863–3868 (2005).

65. C. Zelano *et al.*, Nasal respiration entrains human limbic oscillations and modulates cognitive function. *J. Neurosci.* **36**, 12448–12467 (2016).

66. J. P. Royet, J. Pager, Olfactory bulb responsiveness to an aversive or novel food odor in; the unrestrained rat. *Brain Res. Bull.* **7**, 375–378 (1981).

67. J. Pager, I. Giachetti, A. Holley, J. Le Magnen, A selective control of olfactory bulb electrical activity in relation to food deprivation and satiety in rats. *Physiol. Behav.* **9**, 573–579 (1972).

68. R. Hermer-Vazquez, L. Hermer-Vazquez, S. Srinivasan, J. K. Chapin, Beta- and gamma-frequency coupling between olfactory and motor brain regions prior to skilled, olfactory-driven reaching. *Exp. Brain Res.* **180**, 217–235 (2007).

69. R. M. Khan *et al.*, Predicting odor pleasantness from odorant structure: Pleasantness as a reflection of the physical world. *J. Neurosci.* **27**, 10015–10023 (2007).

70. L. Secundo, K. Snitz, N. Sobel, The perceptual logic of smell. *Curr. Opin. Neurobiol.* **25**, 107–115 (2014).

71. J. Poncelet *et al.*, Semantic knowledge influences prewired hedonic responses to odors. *PLoS One* **5**, e13878 (2010).

72. M. Bensafi, F. Rinck, B. Schaal, C. Rouby, Verbal cues modulate hedonic perception of odors in 5-year-old children as well as in adults. *Chem. Senses* **32**, 855–862 (2007).

73. N. Mandairon, J. Poncelet, M. Bensafi, A. Didier, Humans and mice express similar olfactory preferences. *PLoS One* **4**, e4209 (2009).

Iravani et al.
The human olfactory bulb processes odor valence representation and cues motor avoidance behavior

PNAS | 11 of 12
https://doi.org/10.1073/pnas.2101209118

74. P. Joussain, A. Chakirian, F. Kermen, C. Rouby, M. Bensafi, Physicochemical influence on odor hedonics: Where does it occur first? *Commun. Integr. Biol.* **4**, 563–565 (2011).

75. A. Keller *et al.*, Predicting human olfactory perception from chemical features of odor molecules. *Science* **355**, 820–826 (2017).

76. C. Sezille *et al.*, Dissociated neural representations induced by complex and simple odorant molecules. *Neuroscience* **287**, 23–31 (2015).

77. P. Gupta, D. F. Albeanu, U. S. Bhalla, Olfactory bulb coding of odors, mixtures and sniffs is a linear sum of odor time profiles. *Nat. Neurosci.* **18**, 272–281 (2015).

78. M. A. Patterson, S. Lagier, A. Carleton, Odor representations in the olfactory bulb evolve after the first breath and persist as an odor afterimage. *Proc. Natl. Acad. Sci. U.S.A.* **110**, E3340–E3349 (2013).

79. G. Kobal *et al.*, Multicenter investigation of 1,036 subjects using a standardized method for the assessment of olfactory function combining tests of odor identification, odor discrimination, and olfactory thresholds. *Eur. Arch. Otorhinolaryngol.* **257**, 205–211 (2000).

80. R. D. Pascual-Marqui *et al.*, Assessing interactions in the brain with exact low-resolution electromagnetic tomography. *Philos. Trans.- Royal Soc., Math. Phys. Eng. Sci.* **369**, 3768–3784 (2011).

81. R. Oostenveld, P. Fries, E. Maris, J.-M. Schoffelen, FieldTrip: Open source software for advanced analysis of MEG, EEG, and invasive electrophysiological data. *Comput. Intell. Neurosci.* **2011**, 156869 (2011).

82. F. Tadel, S. Baillet, J. C. Mosher, D. Pantazis, R. M. Leahy, Brainstorm: A user-friendly application for MEG/EEG analysis. *Comput. Intell. Neurosci.* **2011**, 879716 (2011).

83. N. N. Oosterhof, A. C. Connolly, J. V. Haxby, CoSMoMVPA: Multi-modal multivariate pattern analysis of neuroimaging data in Matlab/GNU octave. *Front. Neuroinform.* **10**, 27 (2016).

84. M. Rubinov, O. Sporns, Weight-conserving characterization of complex functional brain networks. *Neuroimage* **56**, 2068–2079 (2011).

85. M. Rubinov, O. Sporns, Complex network measures of brain connectivity: Uses and interpretations. *Neuroimage* **52**, 1059–1069 (2010).